# Conductance Switching in Liquid Crystal-Inspired Self-Assembled Monolayer Junctions

Julian M. Dlugosch, Henning Seim, Achyut Bora, Takuya Kamiyama, Itai Lieberman, Falk May, Florian Müller-Plathe, Alexei Nefedov, Saurav Prasad, Sebastian Resch, Kai Saller, Christian Seim, Maximilian Speckbacher, Frank Voges, Marc Tornow,* and Peer Kirsch*

ABSTRACT: We present the prototype of a ferroelectric tunnel junction (FTJ), which is based on a self assembled monolayer (SAM) of small, functional molecules. These molecules have a structure similar to those of liquid crystals, and they are embedded between two solid state electrodes. The SAM, which is deposited through a short sequence of simple fabrication steps, is extremely thin (3.4 ± 0.5 nm) and highly uniform. The functionality of the FTJ is ingrained in the chemical structure of the SAM components: a conformationally flexible dipole that can be reversibly reoriented in an electrical field. Thus, the SAM acts as an

electrically switchable tunnel barrier. Fabricated stacks of $Al/Al_2O_3/SAM/Pb/Ag$ with such a polar SAM show pronounced hysteretic, reversible conductance switching at voltages in the range of $\pm 2-3$ V, with a conductance ratio of the low and the high resistive states of up to 100. The switching mechanism is analyzed using a combination of quantum chemical, molecular dynamics, and tunneling resistance calculation methods. In contrast to more common, inorganic material based FTJs, our approach using SAMs of small organic molecules allows for a high degree of functional complexity and diversity to be integrated by synthetic standard methods, while keeping the actual device fabrication process robust and simple. We expect that this technology can be further developed toward a level that would then allow its application in the field of information storage and processing, in particular for in memory and neuromorphic computing architectures.
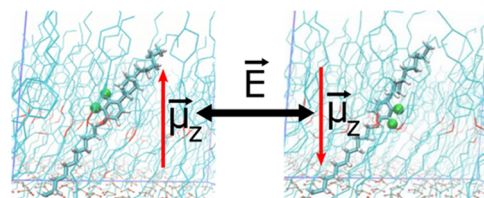
KEYWORDS: liquid crystals, self assembled monolayer, resistive switching, molecular electronics, tunnel junction

INTRODUCTION

It is expected that the global information and communications technology (ITC) infrastructure will consume 21% (8000 TWh) of the total electricity production in 2031.[1] Emerging technologies such as cloud computing, the Internet of Things (IoT), and machine learning add to an ever increasing demand for cheap, low power, and fast processing of large amounts of data.[2,3] To provide energetically sustainable ITC platforms in the future while still increasing computational power, new, more power efficient paradigms such as in memory and neuromorphic computing are currently explored.[4] Even though most of these novel concepts can be implemented in CMOS technology, they require a large number of transistors and passive components, consuming considerable energy and space on a chip. Hence, a power and area efficient physical implementation requires the simultaneous development of advanced materials and devices.[5,6] One particularly promising hardware platform currently being explored for the afore mentioned emerging computational paradigms is memristive two terminal devices based on ferroelectric tunnel junctions (FTJs).[7]

Typically, the active components of FTJs are ultrathin layers (<4 nm) of ferroelectric inorganic insulators (e.g., HfO_2)[8] or fluoropolymers (e.g., VDF TrFE copolymer).[9,10] Smaller molecular systems providing a memristive or conductance switching functionality rely either on a redox process[11] or on using a larger bulk of the material that precludes the operation as a tunneling device.[12]

Here, we present a concept for SAM based memory devices composed of liquid crystal molecules,[13,14] which are designed not to undergo any kind of chemical reaction during operation, i.e., no bond breaking, change of redox state, or electronic excitation. This may potentially minimize degradation and increase the stability of the resulting device. Structurally, the SAM molecules feature an integrated, conformationally flexible dipolar group. This dipolar group enables an electrical field driven conformational reorientation of the molecule leading to significant, remanent (up to 15−30 min) changes in its conductive state. For device fabrication, the molecules are anchored to a bottom electrode via conformationally flexible
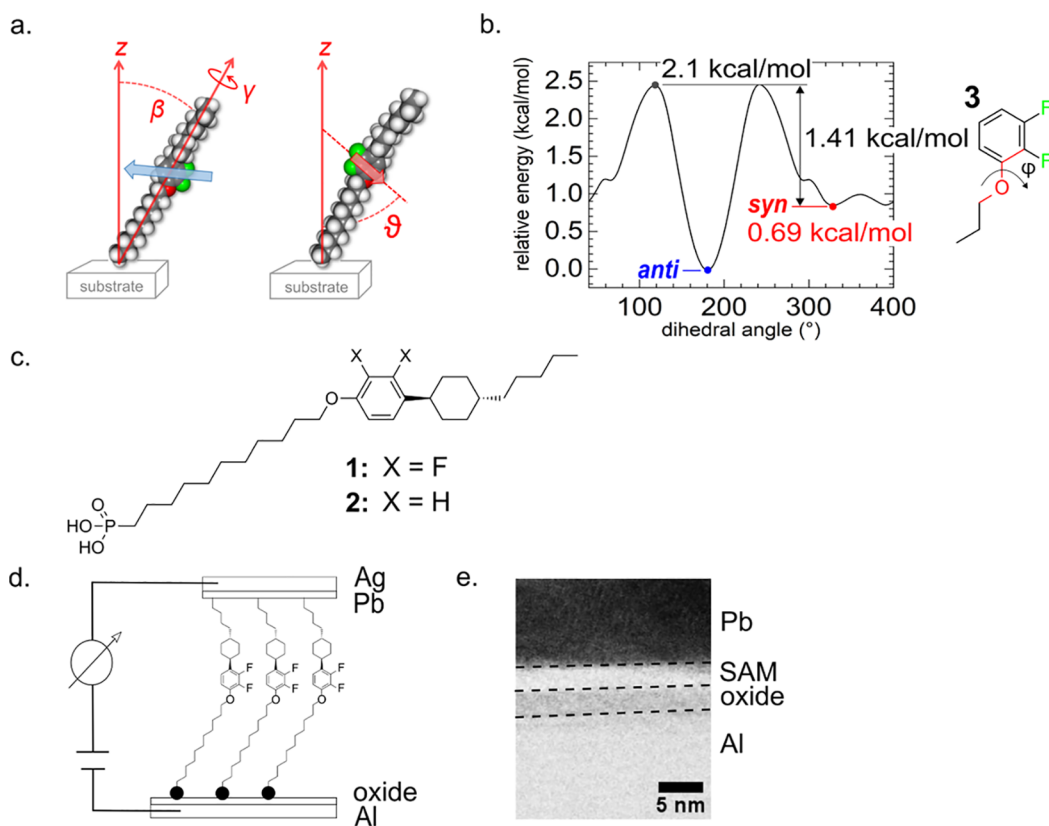
Figure 1. (a) Concept of molecule **1** switching from *anti* (blue) to *syn* (red) conformation: electrical dipole orientation (bold blue/red arrow with dipole pointing from negative to positive charge) with respect to the surface normal z (angle ϑ) is strongly governed by the orientation of the carbon−fluorine bond (fluorine depicted in green). The dipole is utilized to induce orientation changes by coupling to an applied electrical field. Molecular orientation is described by tilt angle β for the long molecular axis, the orientation of the aromatic moiety is defined by its normal vector (here, perpendicular to the paper plane, therefore not depicted) versus z (angle α), and the rotation around the long molecular axis is described by angle γ. *Anti* conformer **1** (left): $\beta = 32°$, $\vartheta = 89°$, $\mu_{tot} = 3.26$ D, $\mu_z = 0.02$ D; *syn* conformer **1** (right): $\beta = 35°$, $\vartheta = 51°$, $\mu_{tot} = 1.50$ D, $\mu_z = -0.71$ D. (b) Calculated conformational energy scan for the rotation of simplified model compound **3** around dihedral angle φ. The annotated values at selected extrema differ from the scale bar of the graph since at these points of interest an additional zero point energy correction was performed, see also the "Computational Chemistry" section in the Supporting Information. The intramolecular rotational barrier is low enough to allow essentially unhindered rotation at room temperature (calculated by density functional theory as described in the Methods section). In equilibrium, the *anti* conformer is slightly favored. (c) Structures of the two employed SAM building molecules **1** and **2**. (d) Schematic of the ensemble molecular junction with the self assembled monolayer embedded between aluminum/aluminum oxide and lead/silver solid electrodes. (e) Transmission electron microscopy (TEM) cross sectional image of one of the 15 × 15 μm^2 junctions showing successful top contact formation on top of the SAM. Dashed lines indicate the interfaces of the individual layers.

linkers. The formed SAM is then covered by a conductive top electrode. When cycling the applied voltage across the junction, a pronounced bipolar hysteresis in conductance is observed. Molecular dynamics (MD) simulations support our interpretation that the flexible dipolar units within the SAM would adopt a whole spectrum of adjustable orientations, eventually causing the observed varying currents across the junction.

■ RESULTS AND DISCUSSION

Dipolar Monolayer Junction. The ensemble molecular junctions were practically realized with the SAM embedded between aluminum/aluminum oxide bottom electrodes and lead/silver top electrodes (see Figure 1 and the Supporting Information). The dipolar SAM molecule (chemical design **1**) was inspired by liquid crystals with negative dielectric anisotropy ($\Delta\varepsilon$) that are being used, e.g., in LCD TVs.[13,14] As a covalent anchor to the bottom electrode, a phosphonic acid group was chosen. Both aliphatic and aromatic organo phosphonate SAMs have been widely investigated. They form

stable and structurally well organized layers on a large variety of semiconductor and metal oxides,[15,16] including, in particular, alumina.[17−20] To clean and activate the surface for phosphonate binding, the bottom electrodes were treated with oxygen plasma. Surface functionalization was carried out by immersion of the bottom electrode substrate in a 1 mM solution of **1** in tetrahydrofuran (THF). Finally, the top electrode was applied by physical vapor deposition of lead,[21] followed by a capping layer of silver without breaking the vacuum. The bottom metal layer was structured by lithography and wet etching, whereas the top metal layer was structured through a shadow mask. A cross section of the complete molecular junction is schematically represented in Figure 1d.

In order to investigate whether the proposed switching effect can be attributed to the presence of the polar group, molecular junctions using the nonpolar, nonfluorinated but sterically equivalent phosphonic acid **2** were fabricated under the same conditions as a reference.

Additionally, monolayers of all aforementioned molecules on planar, unstructured aluminum oxide were fabricated and

characterized to verify SAM formation (see the "Fabrication and Characterization of Planar Test Chips" section in the Supporting Information). Atomic force microscopy (AFM) imaging showed a similar surface roughness before and after SAM formation. Static water contact angle (WCA) analysis showed a surface transition from rather hydrophilic (WCA < 90°) before SAM formation to more hydrophobic (WCA > 105°) after SAM formation. Since all molecules under investigation are terminated with a hydrophobic alkyl group, this indicates the formation of SAMs on the hydrophilic aluminum oxide surface. Variable angle spectroscopic ellipsometry shows high sample to sample comparability. TEM images of FIB cut lamellae of complete devices (Al/Al$_2$O$_3$/SAM/Pb/Ag) show a SAM thickness of 3.4 ± 0.5 nm for **1** and **2** (see the Supporting Information, Figure S7).

Synchrotron based X ray photoelectron spectroscopy (XPS) analysis on planar substrates confirmed the successful monolayer formation for both molecules. In addition, near edge X ray absorption spectroscopy (NEXAFS) showed the same orientation of the aromatic plane with its normal vector at an angle of $\alpha = 67 \pm 2°$ to the surface normal (defined as the z direction throughout this paper; see the Supporting Information, Figures S2−S6). All results confirmed the reproducible formation of smooth, surface conforming monolayers without multilayers. The film formation behavior of **1** and **2** is comparable; hence, we anticipate that any differences in electronic device properties would directly relate to molecular structure.

Molecular dynamics (MD) simulations of the SAM agree with the experimentally determined α for a surface density of $n = 3.1$ molecules·nm^{-2}. They also allow deduction of tilt angle β of the long molecular axis (defined as the straight connection between the phosphorus atom of the anchor group and the carbon of the terminal methyl group) with respect to z, yielding $\beta = 37°$ in combination with a rotation angle around the long molecular axis of $\gamma = 50°$ (measured from the tilt plane), see Figure 1a. Here, for simplification, the $\gamma = 90°$ case is shown, implying $\alpha = 90°$ as $\cos(\alpha) = \sin(\beta)\cos(\gamma)$. The average molecular length obtained from the MD simulations measuring the distance between the phosphorus atom and the terminal methyl carbon atom (2.7 nm) is somewhat smaller than the results from transmission electron microscopy (TEM) cross sectional imaging (see also Figures 1e and S7).

Electrical Characterization of Ensemble Molecular Devices. We have electrically characterized ensemble molecular junctions with embedded SAM **1** by applying a voltage to the top versus the bottom contact (Figure 1d) and by varying this voltage in a cyclic manner. Starting from zero, the voltage was first ramped up to 3.0 V at a constant sweep speed of 50 mV·s^{-1}. Having reached this maximum value, the sweep direction was reversed until the maximum voltage of opposite polarity was reached, before sweeping back to zero. Each cycle corresponds to a measurement duration of 4 min. This cycle was then repeated, typically until ten full cycles were complete. As Figure 2a shows, the measured currents rose with applied bias, reaching maximum values of up to 100 nA, which corresponds to a current density of 0.016 A·cm^{-2}. The currents revealed a pronounced hysteresis: depending on sweep direction and history of the junction, a distinct high resistive state (HRS) and low resistive state (LRS) were observed. The different states did not follow an abrupt, digital switching as typically observed in, e.g., electrochemical metallization cells (EMCs). Our ensemble molecular junctions rather showed a
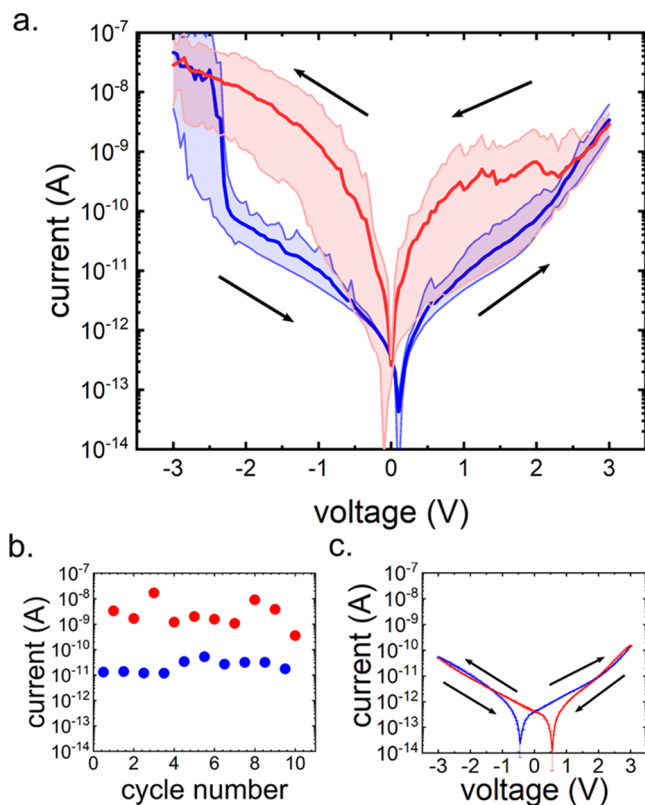

Figure 2. (a) Semilogarithmic representation of the absolute current−voltage (I−V) characteristics of an Al/Al$_2$O$_3$/SAM(**1**)/Pb/Ag, 25 × 25 μm^2 area junction. Bold curves show the average of ten consecutive cycles on this single junction: blue (positive sweep direction) for the HRS and red (negative sweep direction) for the LRS. The thin curves below and above the average are the measured minimum and maximum current traces (envelopes). Black arrows nearby the traces indicate the sweep direction. (b) Currents in HRS and LRS versus the number of sweep cycles extracted from the same junction at reference voltage $V = -1.0$ V indicate good repeatability of the switching process. (c) Reference I−V data for a reference junction containing SAM **2**, showing the average of ten cycles. Blue indicates positive sweep direction, and *red* indicates negative sweep direction. Error bars represent standard deviation and are hardly visible due to low sweep to sweep variability. The offset on the voltage axis can be assigned to capacitive charging currents.

gradual change of resistance with bias voltage. A typical off/on resistance ratio on the order of 10^2 was extracted at a reference bias voltage of −1 V. The repeatability of the switching process of our monolayer junction was probed by cycling the voltage multiple times. Figure 2b illustrates the stable on/off current switching versus the number of cycles, for ten cycles. As we will elaborate in the following, we assign our observed bistable, gradual resistance switching to conformational changes of the embedded molecular dipoles of compound **1**. In fact, the reference junctions containing a SAM of the nonpolar (nonfluorinated) but sterically equivalent reference compound **2** showed no such hysteresis (Figure 2c).

We note that the absolute current for devices showing hysteresis is slightly different for voltages of opposite polarity. For instance, the average rectification ratio $R = |I(-1 \text{ V})|/|I(1 \text{ V})|$ is 1.2 for the HRS and 5.7 for the LRS. This asymmetry may be induced by the aromatic moiety being asymmetrically located along the alkyl backbone, which would lead to an asymmetric energy landscape at voltages of opposite polarity.
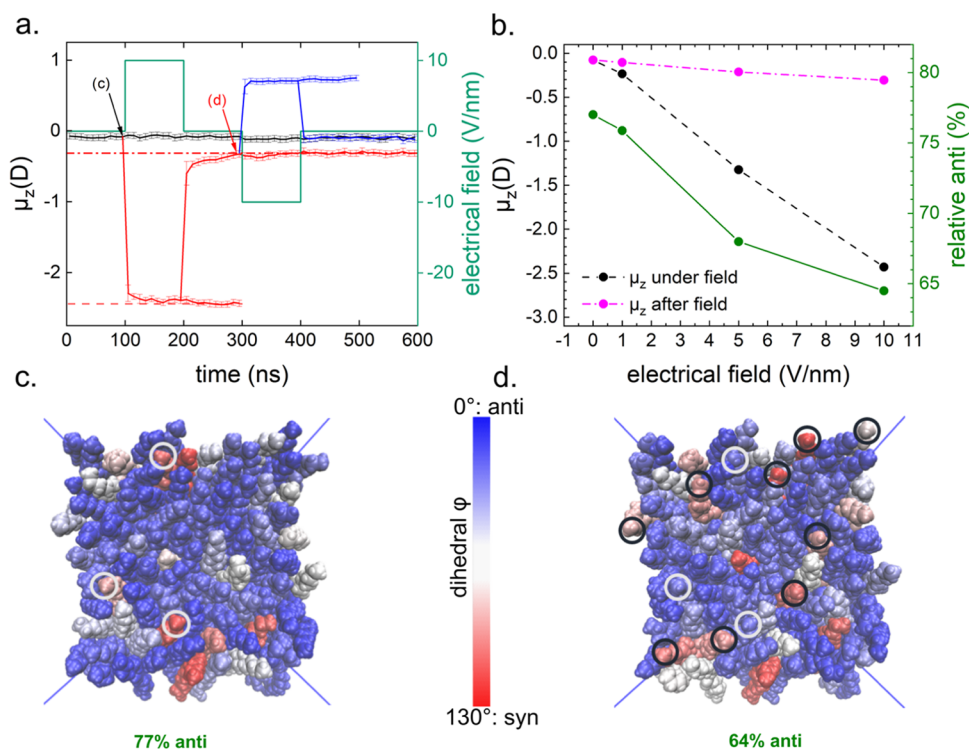
Figure 3. (a) MD simulations of SAM **1**: dipole moment μ_z averaged per molecule (left axis) for electrical field pulses (right axis) over time t (error bars from fluctuations). Black curve: initial state without the field. Red curve (sequence 1): +10 V·nm^{-1} "on" at t = 100 ns and "off" at t = 200 ns until 600 ns. Blue curve (sequence 2): continuing from red at t = 300 ns with −10 V·nm^{-1} and "off" at t = 400 ns, returning to the initial state revealing polarization hysteresis of the red state of $\Delta\mu_z$ = −0.2 D. The green line (sequence 3) marks the full electric field sequence for the latter case. (b) Dipole moment μ_z (left axis) from a similar pulse sequence as in (a), as a function of the z component of the electrical field E_z = 0, 1, 5, 10 V·nm^{-1}. Dashed black line: μ_z under an applied positive field (averaged for 200−300 ns) shows linear behavior, corresponding (for E_z = 10 V· nm^{-1}) to a situation marked by the dashed lower red line in (a). Dash dotted pink and full green line: μ_z and fraction of molecules in the *anti* conformer (right axis), respectively, after the field is off (averaged for 300−400 ns), corresponding to the situation marked by the dash dotted upper red line in (a). (c) Top view at t = 90 ns for the initial state (no field) with molecules colored according to the dihedral angle φ. (d) Same for t = 290 ns after a positive field was applied and turned off, showing that fewer molecules were switched from *syn* to *anti* (light circles in (c) and (d)) than from *anti* to *syn* (dark circles in (d)), resulting in net polarization hysteresis. The diagonal lines in (c) and (d) are the boundaries of the simulation box in the top view.

Others have found that this asymmetric placement can in fact induce rectification with rectification ratios larger than 10^2.[22,23] Further factors, potentially contributing to this asymmetry, may likely be associated with the asymmetric binding of the molecules to either electrode and the presence of a large bandgap oxide only on one side. Here, possible additional surface state charges and interfacial dipoles may result in even more asymmetric potential landscapes.

The hysteresis apparent in Figure 2 was in fact observed for five additional devices of the same junction area. Current density−voltage traces averaged over all six devices indicate low device to device variability, cf. Supporting Information, Figure S8.

Reorientation of Dipolar Molecules in an Electrical Field. To investigate the microscopic mechanism of the observed pronounced hysteresis, we have focused on an anticipated reorientation of the SAM molecular dipoles in the external electric field. Similar switching has been experimen tally observed in a liquid crystalline Langmuir−Blodgett film using an optical method.[24] Electrical field induced monolayer structural changes have been experimentally observed to significantly improve rectification ratios of ferrocene based molecular diodes, well supported by MD simulations.[25] Here, owing to the molecular design of **1**, the fluorine associated local dipole in the z direction may effectively change

depending on the rotation of the 2,3 difluorophenylene unit with respect to the long molecular axis. To result in the disparate, bistable states observable in the electrical data, both dipolar orientations must be somewhat conformationally "locked" in energetic minima. Figure 1b illustrates the potential energy profile calculated by density functional theory (for details, see the Methods section) of an isolated model compound **3** during rotation around the phenolic O−C$_{ar}$ axis (only this conformational environment has a significant influence on dipole orientation), yielding an intramolecular barrier of only 1.41 kcal·mol^{-1} (2.38 kT at 298 K) from *anti* to *syn* and 2.10 kcal·mol^{-1} (3.54 kT) from *syn* to *anti*. This means that for the isolated molecule, relatively unhindered rotation occurs at room temperature. On the other hand, we observed the resistive states to be stable for up to at least 20 min (compare Figure S9). This indicates that the dipole rotation must be hindered by a much higher barrier (>22 kcal·mol^{-1}),[26] presumably due to the additional *inter*molecular steric crowding in the packed SAM.

To investigate whether the dipolar reorientation also takes place within a densely packed SAM where intermolecular forces would shape the energetic landscape, we performed detailed molecular dynamics (MD) simulations. Results of simulations of SAMs of **1** at T = 300 K with a surface density of n = 3.6 molecules·nm^{-2} are shown in Figure 3. They

indicate that a net remanent polarization in the SAM persists even after switching off the external electrical field (for computational details including different surface densities and field strengths, see Table S2 and Figures S11−S17).

To investigate dipole reorientation within the SAM and under the influence of an applied field, we considered several different sequences of applied electrical fields in our MD simulations. We define the direction of the electrical field as in the experiment, i.e., positive, when a positive potential is applied to the top side of the junction. A positive field vector then points toward the substrate, whereas a negative one points away from it. The sequences that were applied are displayed in Figure 3a. In summary, we compared 600 ns without an applied electrical field (sequence 1) to a sequence comprising a 100 ns positive electrical field pulse (sequence 2) and another sequence comprising a 100 ns positive and a 100 ns negative electrical field pulse (sequence 3). Full sequence 3 is displayed as a green line in Figure 3a.

For sequence 1, without an applied electrical field, we have found an average dipole moment in the z direction of $\langle \mu_z \rangle =$ −0.1 D per molecule with roughly 77% of the molecules in the energetically slightly (by 0.69 kcal·mol^{-1}) favored *anti* conformation. This fraction does not significantly change over 600 ns if no field is applied (Figure 3a). We term this state the "initial state." In sequence two, a positive field was applied 100 ns after initial equilibration. We found the dipole moment in the z direction to saturate at μ_z = −2.4 D after 200 ns. One hundred nanoseconds after application of the positive field, 90% of this value was already reached, indicating fast switching. Turning the field off 200 ns after initial equilibration (which corresponds to 100 ns after field application), we observed relaxation of $\langle \mu_z \rangle$ to −0.3 D after ∼100 ns. In this state, 64% of the molecules were found to be in *anti* conformation. This "switched state" is distinct from the initial state and is characterized by 13% fewer molecules in *anti* conformation (see Figure 3c,d for a visual representation of the differences of the SAM in both states). For sequence 3, the SAM was first brought into the same state by first equilibrating for 100 ns and then applying a 100 ns electrical field pulse of positive polarity and letting the system equilibrate once more for 100 ns (no electric field). Then, a field of opposite (negative) polarity was applied for 100 ns. $\langle \mu_z \rangle$ was found to saturate under these conditions after ∼10 ns, at about +0.7 D. Turning the field off again 100 ns later brought the SAM back to a state similar to the initial state: the fraction of molecules in *anti* conformation was found to be 74%, which is close to the initial 77%. In total, the differences between the three sequences revealed that a SAM of molecule **1** can be switched from its initial state with 77% *anti* conformers to a state with 64% *anti* conformers and back to a state with 74% *anti* conformers, simply by applying electrical fields of opposite polarity. Our simulations revealed a total polarization hysteresis between the first two states of $\Delta \mu_z$ = 0.2 D.

This finding is in qualitative agreement with the hysteretic behavior observed in our measured *I−V* characteristics. The experimentally observed LRS state at 0 V (red in Figure 2a) can be associated with the simulated "switched" state at $t > 300$ ns since both have most recently seen a positive field. The experimental HRS state at 0 V corresponds to the state of the SAM after sequence 2 in our simulations since both have most recently seen a negative field. There is, however, a quantitative difference in the applied electric field (z component) $|E_z|$ of a factor of 10 between simulations and experiments. Hence, we have repeated these sequences with smaller absolute field values $|E_z|$ and have found near linear dependencies of the polarization hysteresis on the applied field strength—for the SAM under field as well as after the field has been turned off (Figure 3b). The residual dipole, being a function of the sign and magnitude of the previously applied field, particularly suggests possible future applications of our system in the area of neuromorphic and in memory computing. More details on morphology, density dependence of the observed effects, and electrical switching (including a video) can be found in the Methods section and the Supporting Information.

Tunneling through Asymmetric Barriers of Varying Shape. We propose that the dominant mechanism of charge transport through the oxide/SAM layer is quantum mechanical tunneling. Charge transport by tunneling through double barrier systems, comprising, e.g., an insulating layer (here aluminum oxide) and an organic monolayer (SAM), has been investigated before by us and others.[27,28] Liao et al. as well as Zhang et al. have recently modeled molecular junctions as a series of connected tunnel barriers.[29,30] Here, we assign the pronounced differences in conductance observed for our junctions, at least in part, to differences in nonresonant tunneling transmission through barriers with a different degree of asymmetry, corresponding to the two dipolar conforma tions. This contrasts with the reported finding that different molecular dipoles themselves had only a minor effect on tunneling currents through SAMs.[31,32] In our case, however, the asymmetry of the junction is induced by the structural asymmetry of **1**, resulting in different built in voltage drops across the junction. These depend on dipolar orientation.

The two different, persistent dipole orientations in the SAM lead to two different values of the internal electrostatic potential or voltage drop across the monolayer. For a quantitative estimate of this difference, we have calculated the change in the electronic work function, where a bare (i.e., without top electrode) SAM presents for both dipole orientations. Molecular tailoring of the work function by dipolar SAMs has been widely employed for organic electronic devices.[33] Work function changes up to around ±0.8 eV have been realized.[34,35] Depending on the electrode material, typically thiols (e.g., for gold or III−V semiconductors) or phosphonic acids (e.g., for oxidic materials) have been used as anchor groups, together with a dipolar aromatic or aliphatic moiety.[36−40] For molecule **1** used in our study (without the phosphonate group, to focus solely on the conformationally flexible part of the molecule), we have performed a DFT calculation of the dipole moment.[41−43] The calculation was based on the assumption that the first carbon−hydrogen bond of a simplified analogue of **1** without the phosphonate group is oriented perpendicularly to the electrode surface, leading to α = 90°, β = 33°, and γ = 90° for the optimized geometry. Then, the z component of the total molecular dipole moment (μ_z) switches between 0.02 D (*anti* conformer) and −0.71 D (*syn* conformer), yielding $\Delta \mu_z \approx 0.7$ D. This is slightly larger than observed in the MD simulation (Figure 3a) since, on the one hand, a perfectly oriented single molecule with α = 90° and γ = 90° gives rise to the maximum possible $\Delta \mu_z$. On the other hand, the MD simulation indicates that only 13% of the molecules have been switched permanently. MD provides a slightly larger value $\Delta \mu_z$ per switched molecule (0.2 D/0.13 ≈ 1.5 D), which results from the imperfect representation of conformation dependent dipoles in the MD model (see the "Molecular Dynamics" section in the Supporting Information).

Applying the Helmholtz equation for the shift in the substrate's work function $\Delta\phi$

$$\Delta\phi = \frac{n\mu_z}{\varepsilon_r\varepsilon_0} = \frac{n\mu_{tot}\cos\beta}{\varepsilon_r\varepsilon_0} \qquad (1)$$

with β from Figure 1a and under the assumption that the SAM density is n = 3.1 molecules·nm^{-2} (consistent with the MD and NEXAFS results)[20,44] and that the estimated relative dielectric constant of the SAM is ε_r = 3.0 (see the "Computational Chemistry" section in the Supporting Information) results in a relative difference of 284 meV for the substrate's work function between the two main conformations in the single molecule DFT approach. In the MD approach, after switching a field of 10 V·nm^{-1} on and off again, we obtain $\Delta\phi$ = 81 meV. This value was however found to critically depend on the assumed surface density: if we assume an about 15% higher density of n = 3.6 molecules·nm^{-2} (like in the simulation depicted in Figure 3), the work function is already shifted by 330 meV.

With this and the results of our MD simulations, we have set out to estimate the tunneling currents for both the HRS and LRS based on the available analytical equations for asymmetric tunnel barrier junctions[11,45,46] and to compare them to our experimental findings. All details of the calculations are provided in the "Tunneling Current Estimation" section in the Supporting Information. In brief, we modeled our two barrier system comprising the amorphous aluminum oxide and the organic monolayer as *one* effective tunneling barrier that presents different barrier heights to charge carriers at both contacts. In general, the resulting barrier is of asymmetric, trapezoidal shape. On the aluminum side of the tunneling barrier, the barrier height is kept constant within the approximations of our model. In contrast, on the Pb side, a dipole orientation dependent potential drop $\Delta\phi$ (obtained from the Helmholtz equation) adds to the difference between the Pb work function and the highest occupied molecular orbital (HOMO) of the molecules, cf. Figure S18 for a schematic energy level diagram. All resulting barrier heights enter the formula for the current, as provided by Gruverman et al.,[46] and allow for a calculation of the ratio of currents in LRS or HRS. Since the calculated HOMO of the molecules is considerably closer to the Fermi level than the lowest unoccupied molecular orbital (LUMO), we have included solely hole tunneling in our calculation.[47] At a chosen bias voltage of −1 V, we obtain a current on/off ratio of I_{LRS}/I_{HRS} = 7.2.

This value is notably lower than the one derived from our experiments at the same voltage (ca. 180). We attribute the quantitative difference between theory and experiment in part to the simplifications made in our model, which does not consider charging, interface polarization, and band bending effects. Significantly, however, the analytical formula used for the tunneling current depends sensitively on several critical parameters, which are not well known (effective hole mass m_h^*) or are at best uncertain (molecule density n). For example, assuming an effective hole mass of about m_h^* = $8m_0$ (m_0: electron rest mass) instead of m_0, in our calculations, easily increases the calculated on/off ratio to values comparable to the experimental one, see also Figure S19. Effective hole masses, partially anisotropic, have been reported in a wide range well above or below the electron rest mass for alumina and organic compounds, with $8m_0$ still being in the range of the reported values.[48,49] Assuming a certain, definite

value for our double barrier comprising amorphous alumina and liquid crystal derived molecules, however, would be pure speculation. Therefore, we do not pursue this approach here. We do, however, conclude that our experimental findings are qualitatively well in line with our simplified model, which is fully based on well educated assumptions.

While we assign the described tunneling through asymmetric barriers of different shapes to be the dominating mechanism, we have also considered other contributions accompanying the molecular reorientation, as also investigated in a recent publication by Belding et al.[50] In fact, the conformational change (rotation of the 2,3 difluorophenylene group around the long molecular axis) also affects the electronic orbital structure and thereby the molecular conductance: a single molecule transmission calculation of a simplified analogue of **1** (without phosphonic acid group, see the Supporting Information) using the nonequilibrium Green function[57] indicates a conductance change of about 1 order of magnitude—also significantly less than the experimentally observed value. The results of this calculation are summarized in the Supporting Information, Figure S10. Additional contributions to the observed conductance switching might be attributed to more device related effects such as giant tunnel electroresistance (TER),[51,52] variations in tunneling paths,[18] or steric effects, whereas the polar 2,3 difluorophenylene groups of isolated molecules of **1** show unhindered rotation (activation energy of $E_{A,calc}$ = 1.41 kcal·mol^{-1} from *syn* to *anti* and 2.10 kcal·mol^{-1} from *anti* to *syn*), the crowded steric environment within the SAM is locally increasing the activation barrier of the rotation. The increased activation energy presumably leads to enhanced stability of the different polar states in the range of 15−30 min (E_A > 22 kcal·mol^{-1}).

In summary, our model calculations provide evidence that dipole reorientation within the SAM was mainly responsible for the observed current−voltage hysteresis. Here, the conformational switching in the ensemble SAM would mainly impact the tunnel current through the change in the tunnel barrier, with likely additional contributions through differences in single molecular conductance by the conformation change. The observed remanent polarization can be attributed to roughly 10% of the molecules, retaining their field induced conformation after switching off the field. This fraction increases linearly with the electric field amplitude.

A future full self consistent quantum physical treatment of the charge transport through the SAM's different states described by the results of our molecular dynamics calculations will be based on density functional theory calculations and non linear Green's function methods, possibly even considering collective electrostatic effects. However, these simulations are beyond the scope of our present work that is aimed at introducing the concept of liquid crystal inspired molecules as electrical field controlled molecular switches and at demonstrating their application in ensemble molecular devices with solid contacts.

■ CONCLUSIONS

We have demonstrated repeatable electrical field induced resistance switching due to conformational reorientation of liquid crystal inspired molecules within ensemble molecular solid state devices. The observed pronounced current−voltage hysteresis can be assigned to conformation dependent, remanent tunneling barrier asymmetries and changes in molecular conductance, separating the two polarization states.

Measured off−on resistance ratios were ∼100. This demonstrates the feasibility of exploiting the reorientation of polar molecules in an external field as an electrical field driven switch, opening up an additional route toward future memory and computing devices.

Since the number of distinct states of the SAM is theoretically not limited to just two, the effect presented in this work has the potential to be exploited for applications that require multistate devices, such as neuromorphic or in memory computing as well as the physical implementation of pretrained neural networks for edge computing applications.[53,54]

Future work will address a more in depth understanding of the microscopic charge transport mechanism including the asymmetric nature of the $I−V$ characteristics (partial rectification), supported by additional temperature and frequency dependent (impedance) measurements. Molecular structure optimization and improvements of the device architecture including a lead free replacement of the top electrode material (using, e.g., Ti,[55] Cr, or TiN) shall enable further development of our system toward practical applications, including potentially lower required maximum switching voltages to further enhance device stability. This shall also enable a full benchmarking with the other state of the art resistive switching devices. Future applications may include resistive memories as well as components for neuromorphic and in memory computing.

■ METHODS

Quantum Chemistry. All molecular calculations were done using the B3LYP or M06 2X D3 functionals and the 6 31G(d) basis set as implemented in Gaussian 16, Revision C.01, Version 3 (full citations in the Supporting Information).[56] The B3LYP functional was used to optimize molecular geometries, to calculate molecular dipole moment vectors, and to calculate HOMO and LUMO energies. For the conformational analysis, M06 2X D3 was used. Green's function calculations of the molecular electronic transmission were performed using the Siesta 3.1 package[57] and the GGA PBE functional with a DZ basis set (for full citation, refer to the Supporting Information).

Molecular Dynamics. For the MD of SAM **1**, we used a force field based on optimized potentials for liquid simulations (OPLS) parameters.[58]

To describe the dipole of the conformationally active part of the molecule correctly, we decided to set the atomic charges on the phosphonate group to zero (because it carries a dipole itself). For the remaining atomic charges, we replaced phosphonate with H and took the *anti* conformer geometry optimized by DFT (B3LYP/6 31G (d,p), used partial charges from an ESP fit by the Merz−Kollman method,[59] and imposed a total molecular charge of zero. This approach correctly reproduces molecular dipole vectors as obtained from DFT for the *anti* as well as the *syn* conformer. To complete the force field, we applied an additional torsion potential to reproduce the dihedral scan in Figure 1c). This potential and the atomic partial charges are listed in the Supporting Information.

Unless otherwise stated, the following MD simulations were performed using the GROMACS package with a time step of 0.002 ps with constrained bonds using stochastic velocity rescaling for temperature coupling with a reference temperature of 300 K, a time constant of τ_T = 0.07 ps at 300 K, Berendsen pressure coupling with a reference pressure 1 bar, a time constant of τ_P = 2 ps and compressibility of 4.5×10^{-5} bar^{-1}, and the grid based particle mesh Ewald technique for electrostatic interactions and the Lorentz Berthelot combination rules.[60−63]

To obtain a SAM, we first sampled a single molecule in vacuum starting with the *anti* conformer (now including the phosphonate group) and constraining top and bottom atoms in their respective $x−y−z$ positions to obtain 92 reasonably stretched conformers fulfilling Boltzmann statistics for the φ distributions and an *anti*:*syn* ratio of

roughly 4:1. These 92 molecules were then used to initialize the SAM with a maximum possible density of 3.6 molecules·nm^{-2} while constraining the phosphonate oxygens in the $x−y$ plane using the Packmol program package.[64]

We then equilibrated the SAM for 20 ns using an isothermal−isobaric (NPT) simulation with anisotropic pressure coupling while constraining the phosphonate oxygens in the $x−y$ plane, resulting in a density of n = 3.6 molecules·nm^{-2}. Equilibration was monitored using the total energy and surface density, which were converged to within 1%. Lower densities and their impact on morphology (α, β, and γ from Figure 1a) and switching behavior were studied by increasing the van der Waals radius of the phosphonate oxygens only during this equilibration phase (see the Supporting Information).

To prevent the molecules from aligning completely when electrical fields are applied, we then took the equilibrated SAM and constrained the three phosphonate oxygens as well as the top carbon in their respective $x−y−z$ positions during all following production runs displayed in Figure 3a. The initial state (black) is shown to be stable over 600 ns and we have also confirmed that preparing larger systems with up to 1000 molecules in the same way as described above, as well as putting a free floating graphene sheet on top of the SAM instead of constraining the top carbon atom, yields similar switching behaviors (data not shown).

Sample Fabrication. Ensemble molecular junctions were fabricated utilizing common fabrication schemes. First, smooth silicon substrates covered with thermal oxide were coated with aluminum via physical vapor phase deposition. The bottom electrodes were then structured using common lithographic procedures and KOH etching. Samples were afterward thoroughly cleaned in acetone and isopropanol before they were treated with an oxygen plasma. Samples were then immersed in 1 mM solutions of the SAM compounds outlined above in THF in completely filled and sealed vials. After 72 h, the samples were heated and rinsed with THF. A shadow mask was then aligned to the substrate using a custom made shadow mask alignment kit, and the top electrode was applied through physical vapor phase deposition of lead and silver, without breaking the vacuum in between. Details of the process can be found in the Supporting Information.

■ AUTHOR INFORMATION

Corresponding Authors

Marc Tornow − *Molecular Electronics, Technical University of Munich, 85748 Garching, Germany; Fraunhofer Research Institution for Microsystems and Solid State Technologies (EMFT), 80686 München, Germany;* ⊙ orcid.org/0000 0002 1860 2769; Email: tornow@tum.de

Peer Kirsch − *Electronics R&D, Merck KGaA, 64293 Darmstadt, Germany; Institute of Materials Science, Technical University of Darmstadt, 64297 Darmstadt, Germany; Freiburg Materials Research Center (FMF), Albert Ludwig University Freiburg, 79104 Freiburg, Germany;* ⊙ orcid.org/0000 0002 9024 7933; Email: peer.kirsch@merckgroup.com

Authors

Julian M. Dlugosch − *Molecular Electronics, Technical University of Munich, 85748 Garching, Germany*

Henning Seim − *Electronics R&D, Merck KGaA, 64293 Darmstadt, Germany*

Achyut Bora − *Molecular Electronics, Technical University of Munich, 85748 Garching, Germany*

Takuya Kamiyama − *Molecular Electronics, Technical University of Munich, 85748 Garching, Germany*

Itai Lieberman − *Electronics R&D, Merck KGaA, 64293 Darmstadt, Germany*

Falk May − *Electronics R&D, Merck KGaA, 64293 Darmstadt, Germany*

Florian Müller Plathe − *Eduard Zintl Institute of Inorganic and Physical Chemistry, Technical University of Darmstadt, 64287 Darmstadt, Germany;* ⊙ orcid.org/0000 0002 9111 7786

Alexei Nefedov − *Institute of Functional Interfaces, Karlsruhe Institute of Technology (KIT), 76344 Eggenstein Leopoldshafen, Germany;* ⊙ orcid.org/0000 0003 2771 6386

Saurav Prasad − *Eduard Zintl Institute of Inorganic and Physical Chemistry, Technical University of Darmstadt, 64287 Darmstadt, Germany;* ⊙ orcid.org/0000 0002 2970 7013

Sebastian Resch − *Electronics R&D, Merck KGaA, 64293 Darmstadt, Germany;* ⊙ orcid.org/0000 0002 0513 6092

Kai Saller − *Molecular Electronics, Technical University of Munich, 85748 Garching, Germany*

Christian Seim − *Xploraytion GmbH, 10625 Berlin, Germany*

Maximilian Speckbacher − *Molecular Electronics, Technical University of Munich, 85748 Garching, Germany*

Frank Voges − *Electronics R&D, Merck KGaA, 64293 Darmstadt, Germany*

Notes

The authors declare no competing financial interest.

◼ ABBREVIATIONS

AFM, atomic force microscopy
DFT, density functional theory
HOMO, highest occupied molecular orbital
HRS, high resistive state
LUMO, lowest unoccupied molecular orbital
LRS, low resistive state
MD, molecular dynamics
NEXAFS, near edge X ray absorption spectroscopy
NPT, isothermal−isobaric
OPLS, optimized potentials for liquid simulations
SAM, self assembled monolayer
TEM, transmission electron microscopy
TER, tunneling electroresistance
WCA, water contact angle

◼ REFERENCES

(1) Jones, N. The Information Factories. *Nature* **2021**, *589*, 163−166.

(2) Arshad, R.; Zahmoor, S.; Shah, M. A.; Wahid, A.; Yu, H. Green IoT: An Investigation on Energy Saving Practices for 2020 and Beyond. *IEEE Access* **2017**, *5*, 15667−15681.

(3) Zhang, Z.; Wang, Z.; Shi, T.; Bi, C.; Rao, F.; Cai, Y.; Liu, Q.; Wu, H.; Zhou, P. Memory materials and devices: From Concept to Application. *InfoMat* **2020**, *2*, 261−290.

(4) Prezioso, M.; Merrikh Bayat, F.; Hoskins, B. D.; Adam, G. C.; Likharev, K. K.; Strukov, D. B. Training and Operation of an Integrated Neuromorphic Network Based on Metal Oxide Mem ristors. *Nature* **2015**, *521*, 61−64.

(5) Meijer, G. I. Materials Science. Who Wins the Nonvolatile Memory Race? *Science* **2008**, *319*, 1625−1626.

(6) Williams, R. S. What's Next? [The end of Moore's law]. *Comput. Sci. Eng.* **2017**, *19*, 7−13.

(7) Garcia, V.; Bibes, M. Ferroelectric Tunnel Junctions for Information Storage and Processing. *Nat. Commun.* **2014**, *5*, No. 4289.

(8) Hsain, H. A.; Lee, Y.; Materano, M.; Mittmann, T.; Payne, A.; Mikolajick, T.; Schroeder, U.; Parsons, G. N.; Jones, J. L. Many Routes to Ferroelectric HfO_2: A Review of Current Deposition Methods. *J. Vac. Sci. Technol. A* **2022**, *40*, No. 010803.

(9) Tian, B. B.; Wang, J. L.; Fusil, S.; Liu, Y.; Zhao, X. L.; Sun, S.; Shen, H.; Lin, T.; Sun, J. L.; Duan, C. G.; Bibes, M.; Barthélémy, A.; Dkhil, B.; Garcia, V.; Meng, X. J.; Chu, J. H. Tunnel Electroresistance Through Organic Ferroelectrics. *Nat. Commun.* **2016**, *7*, No. 11502.

(10) Mai, M.; Ke, S.; Lin, P.; Zeng, X. Ferroelectric Polymer Thin Films for Organic Electronics. *J. Nanomater.* **2015**, *2015*, No. 812538.

(11) Han, Y.; Nickle, C.; Zhang, Z.; Astier, H. P. A. G.; Duffin, T. J.; Qi, D.; Wang, Z.; del Barco, E.; Thompson, D.; Nijhuis, C. A. Electric Field Driven Dual Functional Molecular Switches in Tunnel Junctions. *Nat. Mater.* **2020**, *19*, 843−848.

(12) Miyazaki, T.; Shoji, Y.; Ishiwari, F.; Kajitani, T.; Fukushima, T. Design of a Molecular Memory Element with an Alternating Circular Array of Dipolar Rotors and Rotation Suppressors. *Chem. Sci.* **2020**, *11*, 8388−8393.

(13) Kirsch, P.; Bremer, M. Nematic Liquid Crystals for Active Matrix Displays: Molecular Design and Synthesis. *Angew. Chem., Int. Ed.* **2000**, *39*, 4216−4235.

(14) Bremer, M.; Kirsch, P.; Klasen Memmer, M.; Tarumi, K. The TV in Your Pocket: Development of Liquid Crystal Materials for the New Millennium. *Angew. Chem., Int. Ed.* **2013**, *52*, 8880−8896.

(15) Ma, H.; Acton, O.; Hutchins, D. O.; Cernetic, N.; Jen, A. K. Y. Multifunctional Phosphonic Acid Self Assembled Monolayers on Metal Oxides as Dielectrics, Interface Modification Layers and Semiconductors for Low Voltage High Performance Organic Field Effect Transistors. *Phys. Chem. Chem. Phys.* **2012**, *14*, 14110−14126.

(16) Cattani Scholz, A. Functional Organophosphonate Interfaces for Nanotechnology: A Review. *ACS Appl. Mater. Interfaces* **2017**, *9*, 25643−25655.

(17) Pathak, A.; Bora, A.; Braunschweig, B.; Meltzer, C.; Yan, H.; Lemmens, P.; Daum, W.; Schwartz, J.; Tornow, M. Nanocylindrical Confinement Imparts Highest Structural Order in Molecular Self Assembly of Organophosphonates on Aluminum Oxide. *Nanoscale* **2017**, *9*, 6291−6295.

(18) Pathak, A.; Bora, A.; Liao, K. C.; Schmolke, H.; Jung, A.; Klages, C. P.; Schwartz, J.; Tornow, M. Disorder Derived, Strong Tunneling Attenuation in Bis Phosphonate Monolayers. *J. Phys.: Condens. Matter* **2016**, *28*, No. 094008.

(19) Pellerite, M. J.; Dunbar, T. D.; Boardman, L. D.; Wood, E. J. Effects of Fluorination on Self Assembled Monolayer Formation from

Alkanephosphonic Acids on Aluminum: Kinetics and Structure. *J. Phys. Chem. B* **2003**, *107*, 11726−11736.

(20) Wan, X.; Lieberman, I.; Asyuda, A.; Resch, S.; Seim, H.; Kirsch, P.; Zharnikov, M. Thermal Stability of Phosphonic Acid Self Assembled Monolayers on Alumina Substrates. *J. Phys. Chem. C* **2020**, *124*, 2531−2542.

(21) Lovrinčić, R.; Kraynis, O.; Har Lavan, R.; Haj Yahya, A. E.; Li, W.; Vilan, A.; Cahen, D. A New Route to Nondestructive Top Contacts for Molecular Electronics on Si: Pb Evaporated on Organic Monolayers. *J. Phys. Chem. Lett.* **2013**, *4*, 426−430.

(22) Yoon, H. J.; Liao, K. C.; Lockett, M. R.; Kwok, S. W.; Baghbanzadeh, M.; Whitesides, G. M. Rectification in Tunneling Junctions: 2,2′ Bipyridyl Terminated n Alkanethiolates. *J. Am. Chem. Soc.* **2014**, *136*, 17155−17162.

(23) Kang, H.; Kong, G. D.; Byeon, S.; Yang, S.; Kim, J. W.; Yoon, H. J. Interplay of Fermi Level Pinning, Marcus Inverted Transport, and Orbital Gating in Molecular Tunneling Junctions. *J. Phys. Chem. Lett.* **2020**, *11*, 8597−8603.

(24) Tabe, Y.; Yamamoto, T.; Nishiyama, I.; Yoneya, M.; Yokoyama, H. Ferroelectric Nematic Monolayer. *Jpn. J. Appl. Phys.* **2003**, *42*, L406−L409.

(25) Chen, X.; Roemer, M.; Yuan, L.; Du, W.; Thompson, D.; del Barco, E.; Nijhuis, C. A. Molecular diodes with rectification ratios exceeding 10^5 driven by electrostatic interactions. *Nat. Nanotechnol.* **2017**, *12*, 797−803.

(26) Oki, M. Recent Advances in Atropisomerism. In *Topics in Stereochemistry* Eliel, E. L.; Allinger, N. L.; Wilen, S. H., Eds.; John Wiley & Sons: New York, 1983; Vol. 14, pp 1−82.

(27) Bora, A.; Pathak, A.; Liao, K. C.; Vexler, M. I.; Kuligk, A.; Cattani Scholz, A.; Meinerzhagen, B.; Abstreiter, G.; Schwartz, J.; Tornow, M. Organophosphonates as Model System for Studying Electronic Transport through Monolayers on SiO_2/Si Surfaces. *Appl. Phys. Lett.* **2013**, *102*, No. 241602.

(28) Akkerman, H. B.; De Boer, B. Electrical Conduction through Single Molecules and Self Assembled Monolayers. *J. Phys.: Condens. Matter* **2008**, *20*, No. 013001.

(29) Liao, K. C.; Hsu, L. Y.; Bowers, C. M.; Rabitz, H.; Whitesides, G. M. Molecular Series Tunneling Junction. *J. Am. Chem. Soc.* **2015**, *137*, 5948−5954.

(30) Zhang, Y.; Soni, S.; Krijger, T. L.; Gordiichuk, P.; Qiu, X.; Ye, G.; Jonkman, H. T.; Herrmann, A.; Zojer, K.; Zojer, E.; Chiechi, R. C. Tunneling Probability Increases with Distance in Junctions Compris ing Self assembled Monolayers of Oligothiophenes. *J. Am. Chem. Soc.* **2018**, *140*, 15048−15055.

(31) Yoon, H. J.; Bowers, C. M.; Baghbanzadeh, M.; Whitesides, G. M. The Rate of Charge Tunneling Is Insensitive to Polar Terminal Groups in Self Assembled Monolayers in Ag_{TS} $S(CH_2)_n$ $M(CH_2)_m$ $T//Ga_2O_3$ /EGaIn Junctions. *J. Am. Chem. Soc.* **2014**, *136*, 16−19.

(32) Kovalchuk, A.; Abu Husein, T.; Fracasso, D.; Egger, D. A.; Zojer, E.; Zharnikov, M.; Terford, A.; Chiechi, R. C. Transition Voltages Respond to Synthetic Reorientation of Embedded Dipoles in Self Assembled Monolayers. *Chem. Sci.* **2016**, *7*, 781−787.

(33) Love, J. C.; Estroff, L. A.; Kriebel, J. K.; Nuzzo, R. G.; Whitesides, G. M. Self Assembled Monolayers of Thiolates on Metals as a Form of Nanotechnology. *Chem. Rev.* **2005**, *105*, 1103−1169.

(34) Ishii, H.; Sugiyama, K.; Ito, E.; Seki, K. Energy Level Alignment and Interfacial Electronic Structures at Organic/Metal and Organic/Organic Interfaces. *Adv. Mater.* **1999**, *11*, 605−625.

(35) De Boer, B.; Hadipour, A.; Mandoc, M. M.; Van Woudenbergh, T.; Blom, P. W. M. Tuning of Metal Work Functions with Self Assembled Monolayers. *Adv. Mater.* **2005**, *17*, 621−625.

(36) Gärtner, M.; Sauter, E.; Nascimbeni, G.; Wiesner, A.; Kind, M.; Werner, P.; Schuch, C.; Abu Husein, T.; Asyuda, A.; Bats, J. W.; Bolte, M.; Zojer, E.; Terford, A.; Zharnikov, M. Self Assembled Monolayers with Distributed Dipole Moments Originating from Bipyrimidine units. *J. Phys. Chem. C* **2020**, *124*, 504−519.

(37) Szwajca, A.; Wei, J.; Schukfeh, M. I.; Tornow, M. Self Assembled Monolayers of Alkyl Thiols on InAs: A Kelvin probe force microscopy study. *Surf. Sci.* **2015**, *633*, 53−59.

(38) Hanson, E. L.; Schwartz, J.; Nickel, B.; Koch, N.; Danisman, N. Bonding Self Assembled, Compact Organophosphonate Monolayers to the Native Oxide Surface of Silicon. *J. Am. Chem. Soc.* **2003**, *125*, 16074−16080.

(39) Ford, W. E.; Abraham, F.; Scholz, F.; Nelles, G.; Sandford, G.; von Wrochem, F. Spectroscopic Characterization of Fluorinated Benzylphosphonic Acid Monolayers on AlOx/Al Surfaces. *J. Phys. Chem. C* **2017**, *121*, 1690−1703.

(40) McClain, W. E.; Florence, P. R.; Shu, A.; Kahn, A.; Schwartz, J. Surface Dipole Engineering for Conducting Polymers. *Org. Electron.* **2013**, *14*, 411−415.

(41) Zhao, Y.; Truhlar, D. G. The M06 Suite of Density Functionals for Main Group Thermochemistry, Thermochemical Kinetics, Noncovalent Interactions, Excited States, and Transition Elements: Two New Functionals and Systematic Testing of Four M06 Class Functionals and 12 Other Functionals. *Theor. Chem. Acc.* **2008**, *120*, 215−241.

(42) Grimme, S.; Antony, J.; Ehrlich, S.; Krieg, H. A Consistent and Accurate Ab Initio Parametrization of Density Functional Dispersion Correction (DFT D) for the 94 Elements H Pu. *J. Chem. Phys.* **2010**, *132*, No. 154104.

(43) Becke, A. D. Density Functional Thermochemistry. III. The Role of Exact Exchange. *J. Chem. Phys.* **1993**, *98*, 5648−5652.

(44) Chen, D.; Wu, H. K. Y.; Naderi Gohar, S.; Wu, Y.; Huang, Y.; Nie, H. Y. An Extremely Rapid Dip Coating Method for Self Assembly of Octadecylphosphonic Acid and Their Thermal Stability on Aluminum Film. *J. Mater. Chem. C* **2014**, *2*, 9941−9948.

(45) Brinkman, W. F.; Dynes, R. C.; Rowell, J. M. Tunneling Conductance of Asymmetrical Barriers. *J. Appl. Phys.* **1970**, *41*, 1915−1921.

(46) Gruverman, A.; Wu, D.; Lu, H.; Wang, Y.; Jang, H. W.; Folkman, C. M.; Zhuravlev, M.; Felker, D.; Rzchowski, M.; Eom, C. B.; Tsymbal, E. Y. Tunneling Electroresistance Effect in Ferroelectric Tunnel Junctions at the Nanoscale. *Nano Lett.* **2009**, *9*, 3539−3543.

(47) Guo, R.; Tao, L.; Li, M.; Liu, Z.; Lin, W.; Zhou, G.; Chen, X.; Liu, L.; Yan, X.; Tian, H.; Tsymbal, E. Y.; Chen, J. Interface Engineered Electron and Hole Tunneling. *Sci. Adv.* **2021**, *7*, No. eabf1033.

(48) Perevalov, T. V.; Gritsenko, V. A.; Kaichev, V. V. Electronic Structure of Aluminum Oxide: Ab Initio Simulations of α and γ Phases and Comparison with Experiment for Amorphous Films. *Eur. Phys. J. Appl. Phys.* **2010**, *52*, 30501.

(49) Hatch, R. C.; Huber, D. L.; Höchst, H. HOMO Band Structure and Anisotropic Effective Hole Mass in Thin Crystalline Pentacene Films. *Phys. Rev. B* **2009**, *80*, No. 081411.

(50) Belding, L.; Root, S. E.; Li, Y.; Park, J.; Baghbanzadeh, M.; Rojas, E.; Pieters, P. F.; Yoon, H. J.; Whitesides, G. M. Conformation, and Charge Tunneling Through Molecules in SAMs. *J. Am. Chem. Soc.* **2021**, *143*, 3481−3493.

(51) Tsymbal, E. Y.; Kohlstedt, H. Tunneling Across a Ferroelectric. *Science* **2006**, *313*, 181−183.

(52) Max, B.; Hoffmann, M.; Mulaosmanovic, H.; Slesazeck, S.; Mikolajick, T. Hafnia Based Double Layer Ferroelectric Tunnel Junctions as Artificial Synapses for Neuromorphic Computing. *ACS Appl. Electron. Mater.* **2020**, *2*, 4023−4033.

(53) Berdan, R.; Marukame, T.; Ota, K.; Yamaguchi, M.; Saitoh, M.; Fujii, S.; Deguchi, J.; Nishi, Y. Low Power Linear Computation Using Nonlinear Ferroelectric Tunnel Junction Memristors. *Nat. Electron.* **2020**, *3*, 259−266.

(54) Serb, A.; Bill, J.; Khiat, A.; Berdan, R.; Legenstein, R.; Prodromakis, T. Unsupervised Learning in Probabilistic Neural Networks with Multi State Metal Oxide Memristive Synapses. *Nat. Commun.* **2016**, *7*, No. 12611.

(55) Dlugosch, J. M.; Devendra, D.; Chryssikos, D.; Artmeier, S.; Speckbacher, M.; Kamiyama, T.; Tornow, M. I.In *Metallic Top Contacts to Self Assembled Monolayers of Aliphatic Phosphonic Acids on Titanium Nitride*, Proceedings of the IEEE Conference on Nano technology, 2020; pp 29−34.

(56) Frisch, M. J.; Trucks, G. W.; Schlegel, H. B.; Scuseria, G. E.; Robb, M. A.; Cheeseman, J. R.; Scalmani, G.; Barone, V.; Petersson, G. A.; Nakatsuji, H.; Li, X.; Caricato, M.; Marenich, A. V.; Bloino, J.; Janesko, B. G.; Gomperts, R.; Mennucci, B.; Hratchian, H. P.; Ortiz, J. V.; Izmaylov, A. F.; Sonnenberg, J. L.; Williams Young, D.; Ding, F.; Lipparini, F.; Egidi, F.; Goings, J.; Peng, B.; Petrone, A.; Henderson, T.; Ranasinghe, D.; Zakrzewski, V. G.; Gao, J.; Rega, N.; Zheng, G.; Liang, W.; Hada, M.; Ehara, M.; Toyota, K.; Fukuda, R.; Hasegawa, J.; Ishida, M.; Nakajima, T.; Honda, Y.; Kitao, O.; Nakai, H.; Vreven, T.; Throssell, K.; Montgomery, J. A., Jr.; Peralta, J. E.; Ogliaro, F.; Bearpark, M. J.; Heyd, J. J.; Brothers, E. N.; Kudin, K. N.; Staroverov, V. N.; Keith, T. A.; Kobayashi, R.; Normand, J.; Raghavachari, K.; Rendell, A. P.; Burant, J. C.; Iyengar, S. S.; Tomasi, J.; Cossi, M.; Millam, J. M.; Klene, M.; Adamo, C.; Cammi, R.; Ochterski, J. W.; Martin, R. L.; Morokuma, K.; Farkas, O.; Foresman, J. B.; Fox, D. J. *Gaussian 16*, revision 01; Gaussian, Inc.: Wallingford, CT, 2016.

(57) Hedström, S.; Matula, A. J.; Batista, V. S. Charge Transport and Rectification in Donor−Acceptor Dyads. *J. Phys. Chem. C* **2017**, *121*, 19053−19062.

(58) Jorgensen, W. L.; Tirado Rives, J. The OPLS [Optimized Potentials for Liquid Simulations] Potential Functions for Proteins, Energy Minimizations for Crystals of Cyclic Peptides and Crambin. *J. Am. Chem. Soc.* **1988**, *110*, 1657−1666.

(59) Besler, B. H.; Merz, K. M.; Kollman, P. A. Atomic Charges Derived from Semiempirical Methods. *J. Comput. Chem.* **1990**, *11*, 431−439.

(60) Lindahl, E.; Hess, B.; van der Spoel, D. GROMACS 3.0: A Package for Molecular Simulation and Trajectory Analysis. *J. Mol. Model.* **2001**, *7*, 306−317.

(61) Bussi, G.; Donadio, D.; Parrinello, M. Canonical Sampling Through Velocity Rescaling. *J. Chem. Phys.* **2007**, *126*, No. 014101.

(62) Berendsen, H. J. C.; Postma, J. P. M.; Van Gunsteren, W. F.; Dinola, A.; Haak, J. R. Molecular Dynamics with Coupling to an External Bath. *J. Chem. Phys.* **1984**, *81*, 3684−3690.

(63) Essmann, U.; Perera, L.; Berkowitz, M. L.; et al. A Smooth Particle Mesh Ewald Method. *J. Chem. Phys.* **1995**, *103*, 8577−8593.

(64) Martínez, L.; Andrade, R.; Birgin, E. G.; Martínez, J. M. PACKMOL: A Package for Building Initial Configurations for Molecular Dynamics Simulations. *J. Comput. Chem.* **2009**, *30*, 2157−2164.

■ NOTE ADDED AFTER ASAP PUBLICATION

This paper was published ASAP on July 1, 2022. Figure 1 was increased in size and additional corrections were made to page five of the document, and the corrected version was reposted on July 1, 2022.